Journal of Solid State Chemistry 186 (2012) 87–93

Contents lists available at SciVerse ScienceDirect

Journal of Solid State Chemistry

journal homepage: www.elsevier.com/locate/jssc

The systems Sr–Zn–{Si,Ge}: Phase equilibria and crystal structure of ternary phases

V.V. Romaka [1], M. Falmbigl, A. Grytsiv, P. Rogl *

Institute of Physical Chemistry, University of Vienna, Währingerstr. 42, A-1090 Wien, Austria

ARTICLE INFO

Article history:
Received 27 September 2011
Received in revised form
24 November 2011
Accepted 26 November 2011
Available online 6 December 2011

Keywords:
Silicides
Germanides
Phase equilibria
Crystal structure
XPD
EPMA

ABSTRACT

Phase relations have been established by electron probe microanalysis (EPMA) and X-ray powder diffraction (XPD) for the Sr-poor part of the ternary systems Sr–Zn–Si at 800 °C and Sr–Zn–Ge at 700 °C. In the Sr–Zn–Si system one new ternary compound $SrZn_{2+x}Si_{2-x}$ ($0 \le x \le 0.45$) with $CeAl_2Ga_2$ structure and a statistical mixture of Zn/Si in the 4*e* site was found. Neither a type-I nor a type-IX clathrate phase was encountered. This system is characterized by formation of two further phases, i.e. $SrZn_{1-x}Si_{1+x}$ with ZrBeSi-type ($0.16 \le x \le 0.22$) and $SrZn_{1-x}Si_{1+x}$ with AlB_2-type ($0.35 \le x \le 0.65$) with a random distribution of Zn/Si atoms in the 2*c* site. For the Sr–Zn–Ge system, the homogeneity regions of the isotypic phases $SrZn_{1-x}Ge_{1+x}$ with ZrBeSi-type ($0 \le x \le 0.17$) and AlB_2-type ($0.32 \le x \le 0.56$), respectively, have been determined. Whereas the germanide $SrZn_{2+x}Ge_{2-x}$ ($CeAl_2Ga_2$-type) is characterized by a homogeneity region ($0 \le x \le 0.5$), the clathrate type-I phase $Sr_8Zn_8Ge_{38}$ shows a point composition.

1. Introduction

Semiconducting clathrates, in general, are promising candidates for new thermoelectric materials. Hitherto many systematic studies of phase relations, crystal structures and physical properties of ternary phases in the systems Ba–*M*–{Si,Ge} with *M*=Mn, Fe, Co, Ni, Cu, Zn, Pd, Ag, Cd, Pt, Au were carried out and showed the presence of thermoelectric clathrate-I phases essentially as solid solutions $Ba_8M_xGe_{46-x-y}\square_y$ of *M*-atoms in binary $Ba_8Ge_{43-x}\square_x$ [1–19]. Although transition metals are involved, the endpoint of the solid solutions coincides in most cases with the so-called Zintl limit near a metal to insulator transition [1–7,9,10]. However, the formation of clathrates in the homologous systems with strontium has hitherto been elucidated only in a few cases. Whereas a clathrate type I phase, $Sr_8Zn_8Ge_{38}$, was defined by neutron powder diffraction [20], no clathrate was encountered in the systems Sr–{Ni,Cu}–Si [21]. The results for $Ba_8M_xGe_{46-x-y}\square_y$ and $Ba_8M_xSi_{46-x}$ have demonstrated [1–19], that physical properties can be shifted from metallic-like to semiconducting behavior via the amount of substituted *M*-atoms. As detailed knowledge on the ternary phase diagrams including formation of ternary phases and their corresponding chemical compositions is required in order to define properly the presence and solubility range of clathrates, the authors will provide results of the investigations on the ternary systems Sr–Zn–Ge and Sr–Zn–Si in the compositional region of the type-I clathrate.

Although no complete phase diagram has been evaluated for the systems Sr–Zn–{Si,Ge} a series of isostructural compounds has been discovered. The crystal structure of SrZnSi was described as ZrBeSi-type [22] and later $SrZn_{1-x}Si_{1+x}$ with AlB_2 type was reported [21]. Similarly $SrZn_2Si_2$ has been determined with $CeAl_2Ga_2$ type [23] and SrZnGe with ZrBeSi-type [24]. However, for none of the aforementioned phases the homogeneity region was defined. In order to assess the formation and region of existence of clathrate-type I phases in the systems Sr–Zn–{Si,Ge}, we have investigated the Sr-poor part of the Sr–Zn–{Si,Ge} systems. The current paper will thus provide information on (i) the phase equilibria in the Sr–Zn–{Si,Ge} systems, (ii) on the crystal structures of ternary compounds in the Sr–Zn–Si system, and will provide (iii) a comparison of the investigated systems and explanations to some structural effects in the ternary phases.

2. Experimental

For sample preparation the following components were used—strontium rods with purity 99.5 mass%, zinc granules (Alfa Aesar, purity > 99.9 mass%; purified in quartz ampoules by heating below the Zn boiling point at 907 °C), germanium and silicon pieces with purity better than 99.999 mass%. Oxygen sensitive strontium was cleaned and weighed under cyclohexane.

* Corresponding author. Fax: +43 1 4277 95245.
E-mail address: peter.franz.rogl@univie.ac.at (P. Rogl).
[1] On leave of absence from Lviv Polytechnic National University, Ukraine.

0022-4596/$ - see front matter © 2011 Elsevier Inc. All rights reserved.
doi:10.1016/j.jssc.2011.11.037

For sample preparation the appropriate amounts of Sr (excess of 3 mass% was used to compensate evaporation losses) and Si/Ge were melted in an electric arc-furnace under Ti-gettered argon with a non-consumable tungsten electrode on a water-cooled copper hearth for two times in order to achieve complete fusion and homogeneity. The obtained ingot was cracked into several pieces and with appropriate amounts of Zn was sealed in an evacuated quartz tube. Each ampoule was heated slowly at a rate of 2 °C/min to 950 °C and maintained at this temperature for 2 days to complete the reaction. After that, the temperature was reduced to 800 °C for Si-containing and 700 °C for Ge-containing samples, which were then annealed for 6 days. Finally the samples were water quenched without breaking the ampoules. Temperatures for the isothermal sections (800 °C for the Si-based and 700 °C for the Ge-based system) were selected close to the solidus in the respective binary boundary systems of Sr–Si and Sr–Ge at the nominal binary clathrate composition $Sr_8(Si,Ge)_{46}$.

X-ray powder diffraction data from the annealed specimens were collected with a Guinier–Huber image plate system (Cu$K\alpha_1$; $8^\circ \le 2\theta \le 100^\circ$). Precise lattice parameters were calculated by least-squares fits to indexed 2θ-values employing Ge (for Si-containing samples) or Si (for Ge-containing samples) as internal standards ($a_{Ge}=0.565791$ nm; $a_{Si}=0.543107$ nm) using the CSD program package [25]. For crystal structure refinements we used the FullProf Suite program [26] and the standardization procedure with program Structure Tidy [27]. The annealed samples were polished using standard procedures and were examined by electron probe microanalysis (EPMA). Chemical composition of phases were determined via a Zeiss Supra 55VP scanning electron microscope operated at 20 kV and equipped with an energy dispersive X-ray (EDX) spectrometer supported by the INCA software (Oxford Instruments). Standard deviations for the chemical compositions gained from EPMA were smaller than ± 1 at%.

3. Binary systems

Both equilibrium diagrams, Zn–Si and Zn–Ge are characterized by a complete insolubility of the components at 700 and 800 °C [28]. The liquid phase extends at 700 and 800 °C over most of the phase diagram Sr–Zn [28], sparing only the compound $SrZn_{13}$. A detailed investigation of the Sr–Si system revealed at 800 °C the existence of Sr_2Si, Sr_5Si_3, $SrSi_2$, and SrSi (α or β modifications depending on the cooling rate) [29].

For the Sr–Ge system at 700 °C [28] the formation of Sr_2Ge, SrGe, and $SrGe_2$ has been reported. Although information on the existence of a Sr_5Ge_3 compound was presented [30], no thermodynamic data were given.

4. Results and discussion

4.1. The ternary system Sr–Zn–Si at 800 °C

On the basis of X-ray analyses and EPMA of 17 samples, phase relations at 800 °C were derived in the isothermal section of the Sr–Zn–Si phase diagram (see Fig. 1). Phase equilibria are characterized by the formation of three ternary phases: τ_1-$SrZn_{2+x}Si_{2-x}$ ($CeAl_2Ga_2$-type), τ_2-$SrZn_{1-x}Si_{1+x}$ (ZrBeSi-type), and τ_3-$SrZn_{1-x}Si_{1+x}$ (AlB_2-type). Crystallographic data are listed in Table 1. Despite the insolubility of components in the binary Zn–Si system, all ternary phases are characterized by homogeneity regions with statistical mixtures of Si and Zn atoms in some of the crystallographic positions. Whereas the existence of the phase τ_3-$SrZn_{1-x}Si_{1+x}$ with AlB_2-type [21] was confirmed and the homogeneity region of $0.35 \le x \le 0.65$ was defined on the basis of EPMA and Rietveld

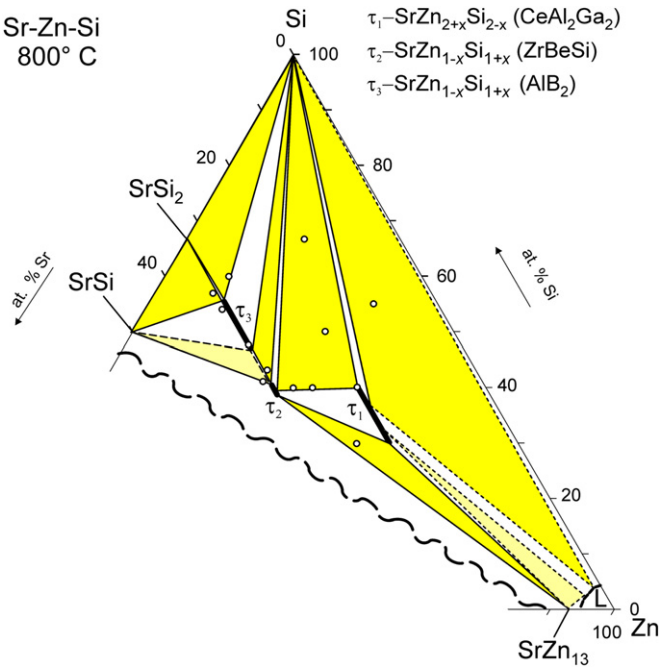

Fig. 1. Isothermal section of the Sr–Zn–Si diagram at 800 °C. Sample positions are indicated by open circles.

refinement data, the ternary phase τ_2-$SrZn_{1-x}Si_{1+x}$, reported at equiatomic composition with the ZrBeSi-type [22], appeared at 800 °C to be shifted along an Sr-isoconcentrate line in the direction of lower Zn content. This deviation from equiatomic composition was confirmed by EPMA and X-ray analysis of the bulk samples (Table 2). A small homogeneity range of $0.16 \le x \le 0.22$ exists at 800 °C, which, however, does not include the 1:1:1 stoichiometric composition SrZnSi earlier reported for a sample heated up to 1000 °C and slowly cooled to room temperature [22]. The phase appeared to be very brittle and rather air-sensitive as it decomposes completely in air within 2–3 days.

The τ_1-$SrZn_{2+x}Si_{2-x}$ phase [23], crystallizing in the $CeAl_2Ga_2$-type, extends within a homogeneity region ranging from $x=0$ to $x \le 0.45$. This phase appeared to be most stable against oxidation among all the ternary compounds in this system. Fig. 2 summarizes microstructures of selected alloys documenting the tie-line distribution at 800 °C for the ternary system Sr–Zn–Si. Interestingly, neither a ternary clathrate of type I ("$Sr_8(Zn,Si)_{46}$") nor of type IX ("$Sr_6(Zn,Si)_{25}$") have been encountered in alloys annealed at 800 °C.

4.2. The ternary system Sr–Zn–Ge at 700 °C

The isothermal section of the Sr–Zn–Ge phase diagram was constructed at 700 °C on the basis of X-ray and EPMA of 13 samples (Fig. 3). In comparison with the Sr–Zn–Si system, the annealing temperature was reduced to 700 °C to avoid liquid regions in the Ge-rich part of the binary and ternary phase diagram. Phase relations in the Sr–Zn–Ge system are characterized by the formation of four ternary phases: τ_1-$SrZn_{2+x}Ge_{2-x}$ ($CeAl_2Ga_2$-type), τ_2-$SrZn_{1-x}Ge_{1+x}$ (ZrBeSi-type), τ_3-$SrZn_{1-x}Ge_{1+x}$ (AlB_2-type) and τ_4-$Sr_8Zn_8Ge_{38}$ (clathrate type I). Crystallographic data are listed in Table 1; results of phase analyses and micrographs are shown in Table 3 and Fig. 4. Similar to the ternary Sr–Zn–Si compounds, all ternary phases with exception of the clathrate phase τ_4 are characterized by homogeneity regions at constant Sr-content but with statistical mixtures of Ge and Zn in

Table 1
Crystallographic data for the Sr–Zn–Si and the Sr–Zn–Ge system.

Compound	Structure type	Space group	Lattice parameters (nm)		Comments
			a, *b*	*c*	
Sr–Zn–Si–system (800 °C)					
τ_1-$SrZn_{2+x}Si_{2-x}$	$CeAl_2Ga_2$	*I*4/*mmm*	0.43262(1)	1.03305(4)	$x=0$[a]
$0 \le x \le 0.45$[a]			0.42714(2)	1.06164(5)	$x=0.45$[a]
τ_2-$SrZn_{1-x}Si_{1+x}$	ZrBeSi	*P*6$_3$/*mmc*	0.42631(1)	0.91084(2)	$x=0.22$[a]
$0.16 \le x \le 0.22$[a]			0.430	0.902	$x=0$ [22]
τ_3-$SrZn_{1-x}Si_{1+x}$	AlB_2	*P*6/*mmm*	0.42307(1)	0.46008(1)	$x=0.35$[a]
$0.35 \le x \le 0.65$[a]			0.41461(1)	0.46965(1)	$x=0.65$[a]
			0.41639	0.46787	[21]
Sr–Zn–Ge-system (700 °C)					
τ_1-$SrZn_{2+x}Ge_{2-x}$	$CeAl_2Ga_2$	*I*4/*mmm*	0.43943(5)	1.06297(1)	$x=0$[a]
$0 \le x \le 0.5$[a]			0.437	1.061	$x=0$ [23]
			0.43587(1)	1.07401(1)	$x=0.5$[a]
τ_2-$SrZn_{1-x}Ge_{1+x}$	ZrBeSi	*P*6$_3$/*mmc*	0.4293(4)	0.934(2)	$x=0$[a]
$0 \le x \le 0.17$[a]			0.4244	0.9126	$x=0$ [24]
τ_3-$SrZn_{1-x}Ge_{1+x}$	AlB_2	*P*6/*mmm*	0.4291(1)	0.4676(6)	$x=0.56$[a]
$0.32 \le x \le 0.56$[a]					
τ_4-$Sr_8Zn_8Ge_{38}$	Clathrate-I	*Pm*-3*n*	1.07074(1)	–	[a]
		Pm-3*n*	1.07044(4)	–	[20]

[a] This work.

Table 2
X-ray phase analysis, lattice parameters and phase composition from EPMA for Sr–Zn–Si alloys annealed at 800 °C; a, b, c, and d refer to the SEM images of Fig. 2.

Nominal composition (at%)			**Phase**	**Structure type**	**Lattice parameter (nm)**			**Composition EPMA (at%)**		
Sr	**Zn**	**Si**			***a***	***b***	***c***	**Sr**	**Zn**	**Si**
40	25	35	$SrZn_{13}$	$NaZn_{13}$	1.22303(6)	–	–	6.4	93.6	–
(a)			τ_1	$CeAl_2Ga_2$	0.42902(1)	–	1.05759(1)	20.6	47.1	32.4
			τ_2	ZrBeSi	0.42844(5)	–	0.8809(2)	31.6	26.3	42.1
20	50	30	$SrZn_{13}$	$NaZn_{13}$	1.21996(7)	–	–	7.7	92.3	–
(b)			τ_1	$CeAl_2Ga_2$	0.42707(2)	–	1.06146(5)	19.1	46.2	34.8
30	10	60	Si	Si	0.54248(1)	–	–	2.8	–	97.2
(c)			$SrSi_2$	$SrSi_2$	0.65300(3)	–	–	33.4	–	66.6
			τ_3	AlB_2	0.41556(1)	–	0.46748(2)	32.8	10.5	56.7
27.0	33.0	40.0	τ_1	$CeAl_2Ga_2$	0.43255(2)	–	1.04196(5)	20.0	43.0	37.0
(d)			Si	Si	0.54417(3)	–	–	–	0.4	99.6

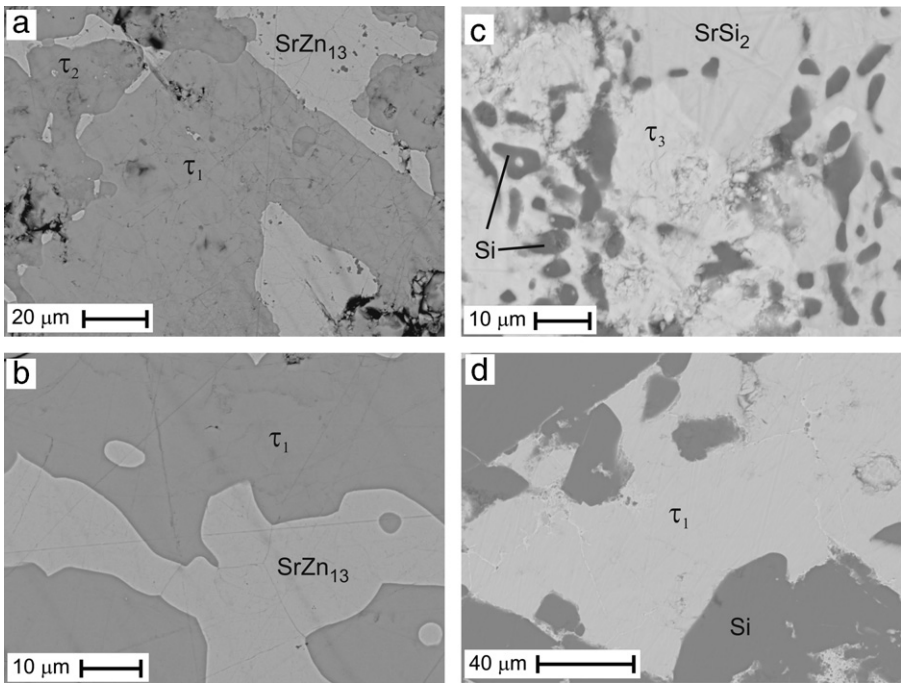

Fig. 2. SEM (backscatter-detector, 20 kV) images of selected samples in the Sr–Zn–Si system (letters on the image correspond to those in Table 2).

crystallographic positions. The clathrate τ_4-phase, for which in a previous report [20] a Zn-content of 7 ± 3 atoms per unit cell at 950 °C was derived from neutron powder diffraction, appeared to adopt at 800 °C the stoichiometry 8:8:38 (according to EPMA data, i.e. with a Zn-content of 8 ± 0.3 atoms/u.c.) with practically identical lattice parameter (Table 1). No solid solution from this ternary clathrate to the hypothetical binary "Sr_8Ge_{46}" was observed. The τ_1-$SrZn_{2+x}Ge_{2-x}$ phase exhibits a homogeneity range $0 \le x \le 0.5$. The homogeneity region of τ_2-$SrZn_{1-x}Ge_{1+x}$ (ZrBeSi-type) extends from the equiatomic composition to $Sr_{33.3}Zn_{27.7}Ge_{39.0}$ ($0 \le x \le 0.17$), whilst the phase τ_3-$SrZn_{1-x}Ge_{1+x}$ (AlB_2-type) extends at 700 °C from $Sr_{33.3}Zn_{22.7}Ge_{44.0}$ to $Sr_{33.3}Zn_{14.7}Ge_{52.0}$ ($0.32 \le x \le 0.56$). The latter two phases τ_2 and τ_3 appeared to be very brittle as well as very sensitive to oxygen or moist air, especially in the presence of $SrGe_2$ and if unprotected, powders change their color within minutes from metallic to brown and finally to orange while decomposing into pure Ge and some unidentified phases. The most stable phases are τ_1 and τ_4. Therefore preparation of specimens for X-ray powder diffraction had to be done either in the glove box under argon or under protective liquids (cyclohexane).

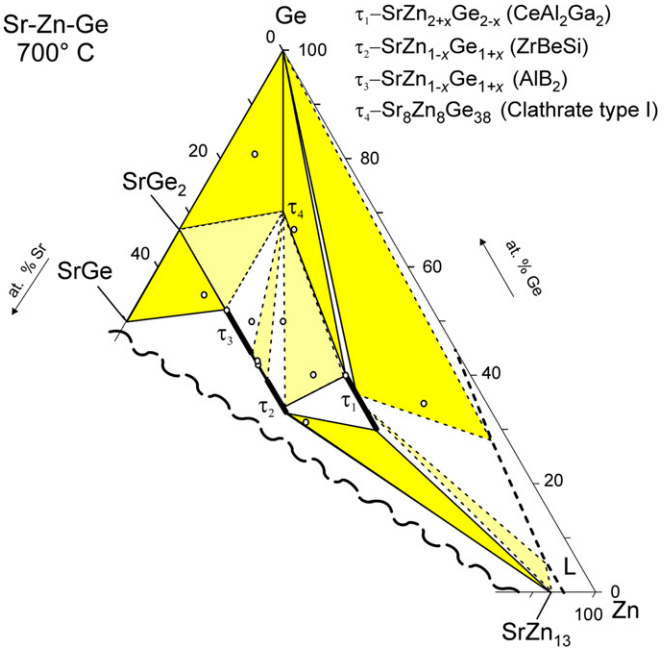

Fig. 3. Isothermal section of the Sr–Zn–Ge diagram at 700 °C. Sample positions are indicated by open circles.

4.3. Comparison of the Sr–Zn–SI and the Sr–Zn–Ge system

Both isothermal sections have many features in common such as (i) formation of isotypic phases with $CeAl_2Ga_2$, ZrBeSi, and AlB_2 structures, (ii) comparable homogeneity regions and (iii) similar phase field distribution. Most interesting is that the presence of Sr in the ternary compounds breaks down the mutual insolubility of Si/Ge and Zn. In all ternary compounds investigated, a random mixture of Zn and Si/Ge atoms in appropriate crystallographic sites is observed. The direction of solubility, however, is different as Si/Ge is partially substituted by Zn for the phases with the $CeAl_2Ga_2$ type and it is vice versa for the phases with AlB_2/ZrBeSi type. Homogeneity regions in the Sr–Zn–Si system are somewhat smaller than those in Sr–Zn–Ge. This could be explained by the size-effect. As Zn atoms are larger than Si this reduces the tolerance limits for substitution in the Sr–Zn–Si structure, whereas Ge and Zn atoms are of almost the same size. Samples in the Sr–Zn–Ge system are much more sensitive to humidity and oxygen than those in Sr–Zn–Si. The main difference between the investigated systems lies in the absence of clathrate formation in the Sr–Zn–Si system. One more important point is that the Sr–Zn–Ge τ_2 homogeneity region at 700 °C includes the equiatomic composition, which is not the case for the Sr–Zn–Si system.

4.4. Structural chemistry

4.4.1. The crystal structure of τ_1-$SrZn_{2+x}Si_{2-x}$

The crystal structure of the phase τ_1-$SrZn_{2+x}Si_{2-x}$ was refined from X-ray powder diffraction data using atom parameters of the $SrZn_2Ge_2$ compound with the $CeAl_2Ga_2$-type [23] as an initial structural model. EPMA results from various samples containing this phase consistently yielded a deviation of up to 9 at% in Zn/Si content from the stoichiometric composition $SrZn_2Si_2$. For this reason three samples with compositions close to the maximum, minimum and intermediate Zn content were selected for Rietveld refinement (Table 4). The compositions refined are very close to those gained from EPMA. As the atomic radius of Zn is somewhat bigger than that of Si, we can expect an enlargement of the unit cell with increasing Zn-content in $SrZn_{2+x}Si_{2-x}$. As shown in Fig. 5 the *c*-parameter increases, whereas the *a*-parameter even reduces slightly, but the cell volume still expands by ~1.5%. A more detailed look on the structural data listed in Table 4 shows that with an increasing amount of Zn-atoms in the 4*e* site

Table 3
X-ray phase analysis, lattice parameters and phase composition from EPMA for Sr-Zn-Ge alloys annealed at 700 °C; a, b, c, d, e, and f refer to the SEM images of Fig. 4.

Nominal composition (at%)			Phase	Structure type	Lattice parameter (nm)			Composition EPMA (at%)		
Sr	Zn	Ge			*a*	*b*	*c*	Sr	Zn	Ge
20.0	40.0	40.0	τ_1	$CeAl_2Ga_2$	0.43580(1)	–	1.07386(4)	19.1	41.1	39.8
(a)										
33.0	33.0	34.0	τ_2	ZrBeSi	0.4293(4)	–	0.934(2)	33.5	34.2	32.3
(b)			SrGe	SrSi	–	–	–	53.5	–	46.5
33.0	15.0	52.0	τ_3	AlB_2	0.4291(4)	–	0.4676(6)	34.4	12.4	53.2
(c)			$SrGe_2$	$BaSi_2$	–	–	–	36.2	–	63.8
14.0	5.0	81.0	τ_4	Clathrate-I	1.07084(1)	–	–	14.4	15.0	70.6
(d)			Ge	Diamond	0.56572(1)	–	–	–	–	100
14.0	5.0	81.0	Ge	Diamond	0.56572(1)	–	–	0	0	100
(e)			$SrGe_2$	$BaSi_2$	–	–	–	32.0	–	68.0
			τ_4	Clathrate-I	1.07084(1)	–	–	14.4	15.0	70.6
14.8	18.5	66.7	Ge	Diamond	0.56572(1)	–	–	0	0	100
(f) 800 °C			τ_4	Clathrate-I	1.0709(2)	–	–	14.7	14.8	70.5
			τ_1	$CeAl_2Ga_2$	0.43943(5)	–	1.06297(1)	20.0	40.8	39.2

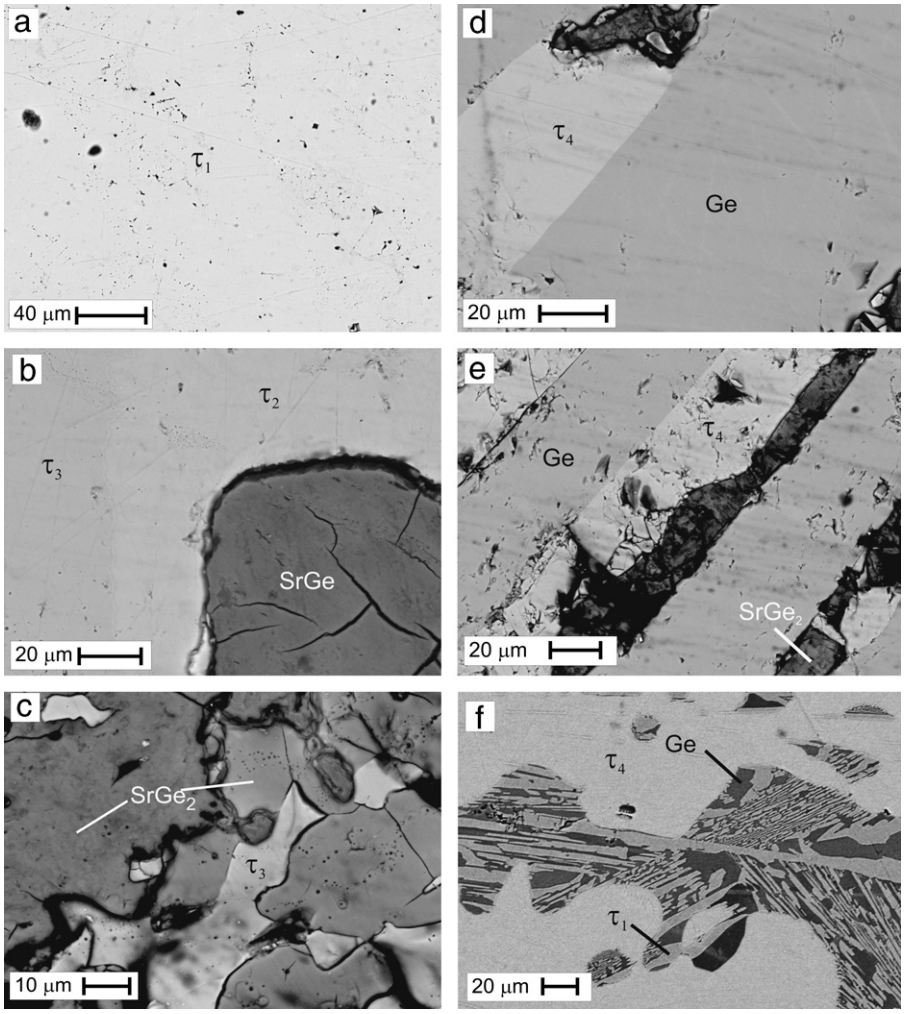

Fig. 4. SEM (backscatter-detector, 20 kV) images of selected samples in the Sr–Zn–Ge system (letters on the image correspond to those in Table 3). Picture f is taken from a sample annealed at 800 °C.

Table 4
X-ray powder Rietveld refinement data for $SrZn_{2+x}Si_{2-x}$.

Parameter/compound	$SrZn_{2+x}Si_{2-x}$	$SrZn_{2+x}Si_{2-x}$	$SrZn_{2+x}Si_{2-x}$
Space group, prototype	*I*4/*mmm*, $CeAl_2Ga_2$	*I*4/*mmm*, $CeAl_2Ga_2$	*I*4/*mmm*, $CeAl_2Ga_2$
Composition, EPMA at%	$Sr_{19.6}Zn_{40.2}Si_{40.2}$	$Sr_{19.9}Zn_{42.5}Si_{37.6}$	$Sr_{20.0}Zn_{48.6}Si_{31.44}$
Composition, XPD at%	$Sr_{20.0}Zn_{42.5(2)}Si_{37.5(2)}$	$Sr_{20.0}Zn_{45.8(1)}Si_{34.2(1)}$	$Sr_{20.0}Zn_{49.9(2)}Si_{30.1(2)}$
a, *c* (nm), Ge standard	0.43262(1); 1.03305(4)	0.43178(1); 1.03980(2)	0.42714(2); 1.06164(5)
Reflections measured	48	48	49
$R_F=\sum\lvert F_o-F_c\rvert/\sum F_o$	0.045	0.020	0.048
$R_I=\sum\lvert I_o-I_c\rvert/\sum I_o$	0.068	0.025	0.064
$R_{wP}=[\sum w_i\lvert y_{oi}-y_{ci}\rvert^2/\sum w_i\lvert y_{oi}\rvert^2]^{1/2}$	0.089	0.038	0.125
$R_P=\sum\lvert y_{oi}-y_{ci}\rvert/\Sigma\lvert y_{oi}\rvert$	0.056	0.023	0.084
$R_e=[(N-P+C)/\sum w_i y_{oi}^2)]^{1/2}$	0.012	0.014	0.018
$\chi^2=(R_{wp}/R_e)^2$	58.3	7.05	47.7
Atom parameters			
Sr in 2*a* (0, 0, 0)	–	–	–
B_{iso} (10^2 nm^2)	1.36(7)	0.52(3)	0.50(6)
Zn in 4*d* (0, 1/2, 1/4)	–	–	–
B_{iso} (10^2 nm^2)	0.86(6)	0.74(2)	1.45(6)
Si/Zn in 4*e* (0, 0, *z*)	$z=0.3862(4)$	$z=0.3853(1)$	$z=0.3840(2)$
Occ. Si/Zn	3.75/0.25(2)	3.42/0.58(1)	3.01/0.99(2)
B_{iso} (10^2 nm^2)	0.74	1.28	1.17

the value of the *z*-coordinate decreases slightly (Fig. 6). This means that the Si–Si distance becomes larger and the bonding between these Si atoms becomes weaker. In the initial (not substituted) compound Si–Si distances are close to the sum of the Si covalent radii and thus the covalent contribution to the Si–Si bond will dominate. When we substitute Si by Zn (maximum 9 at%), the distance between Si/Zn atoms becomes larger and as a result the covalent contribution becomes smaller by

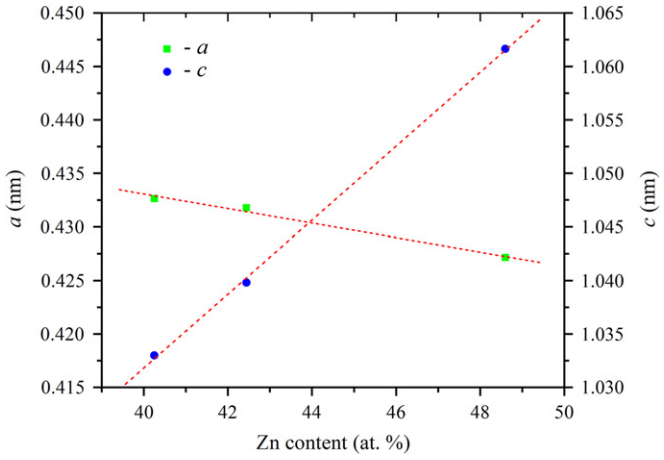

Fig. 5. Lattice parameters versus Zn content for $SrZn_{2+x}Si_{2-x}$ (EPMA data in this work).

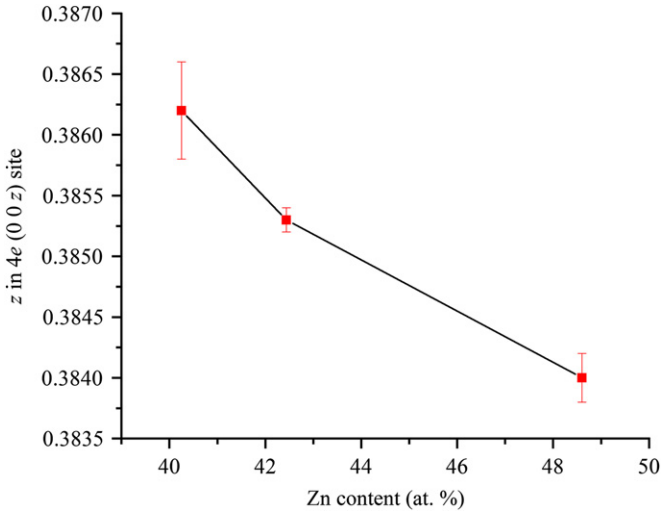

Fig. 6. *z*-coordinate in 4*e* atomic site versus Zn content for $SrZn_{2+x}Si_{2-x}$ (EPMA data).

~13%. Concomitantly the covalent contribution to Sr–Si/Zn bonding increases by ~8%.

For $SrZn_{2+x}Ge_{2-x}$ the same trend in the change of lattice parameters can be observed (Table 1), although due to the much smaller difference in atomic radii of Zn (133.5 pm) and Ge (122.5 pm; Si 117.6 pm) the effect of lowering the *a*- and enlarging the *c*-parameter is not so pronounced. Interestingly practically no volume change is observed. As XPD does not allow a reliable distinction among Zn and Ge, we do not present any details on crystallographic positions.

4.4.2. *The crystal structure of the τ_2/τ_3-$SrZn_{1-x}Si_{1+x}$ phases*

EPMA data of samples between the compositions SrZnSi and $SrSi_2$ showed the presence of two different ternary phases with compositions that could be described by the general formula $SrZn_{1-x}Si_{1+x}$ with $0.16 \le x \le 0.22$ for the τ_2 phase and $0.35 \le x \le 0.65$ for the τ_3 phase. X-ray powder data refinements showed that the τ_2 phase crystallizes with the ZrBeSi type and τ_3 with the AlB_2 type. Refinement of the occupancies revealed a random mixture of Zn/Si atoms in the 2*c* site of both structures (Table 5). As mentioned before and consistent with EPMA data, the refined composition of the τ_2-phase does not include the 1:1:1 stoichiometry. Despite the close relation of crystal structures of these phases the coexistence of both phases is clearly demonstrated in Fig. 7.

The variation of lattice parameters as a function of the Zn-content in $SrZn_{1-x}Si_{1+x}$ is shown in Fig. 8. The ZrBeSi structure type is a superstructure of the AlB_2 type with a two times larger *c* parameter. Taking this fact into account, the *c* parameter for τ_2 is plotted as *c*/2 to compare it with *c* of τ_3. The figure shows that *a* and *c* parameters change gradually and are in good correlation with the data published earlier for the equiatomic composition of τ_2 [22].

5. Conclusions

The isothermal section of the Sr–Zn–Si system was constructed at 800 °C and showed the absence of clathrate phases but the presence of the ternary phases τ_1-$SrZn_{2+x}Si_{2-x}$ ($CeAl_2Ga_2$-type), τ_2-$SrZn_{1-x}Si_{1+x}$ (ZrBeSi-type), and τ_3-$SrZn_{1-x}Si_{1+x}$ (AlB_2-type). The crystal structures of all these silicides were refined and the homogeneity regions due to statistical mixtures of Zn and Si atoms

Table 5
X-ray powder diffraction data for $SrZn_{1-x}Si_{1+x}$ silicides.

Parameter/compound	$SrZn_{1-x}Si_{1+x}$, x=0.22	$SrZn_{1-x}Si_{1+x}$, x=0.36	$SrZn_{1-x}Si_{1+x}$, x=0.67
Space group, Prototype	*P*6$_3$/*mmc*, ZrBeSi	*P*6/*mmm*, AlB_2	*P*6/*mmm*, AlB_2
Composition, EPMA at%	$Sr_{32.5}Zn_{26.0}Si_{41.5}$	$Sr_{33.9}Zn_{20.8}Si_{45.2}$	$Sr_{32.3}Zn_{12.0}Si_{55.7}$
Composition, XPD at%	$Sr_{33.3}Zn_{26.3(2)}Si_{40.4(2)}$	$Sr_{33.3}Zn_{21.3(2)}Si_{45.4(2)}$	$Sr_{33.3}Zn_{11.1(1)}Si_{55.5(1)}$
a; *c* [nm], Ge standard	0.42631(1); 0.91084(2)	0.42307(1); 0.46008(1)	0.41461(1); 0.46965(1)
Reflections measured	44	29	28
$R_F=\sum\|F_o-F_c\|/\sum F_o$	0.020	0.041	0.022
$R_I=\sum\|I_o-I_c\|/\sum I_o$	0.022	0.049	0.038
$R_{wP}=[\sum w_i\|y_{oi}-y_{ci}\|^2/\sum w_i\|y_{oi}\|^2]^{1/2}$	0.058	0.058	0.070
$R_P=\sum\|y_{oi}-y_{ci}\|/\sum\|y_{oi}\|$	0.036	0.036	0.044
$R_e=[(N-P+C)/\sum w_i y_{oi}^2)]^{1/2}$	0.018	0.018	0.036
$\chi^2=(R_{wP}/R_e)^2$	10.2	10.2	3.79
Atom parameters			
	Sr in 2*a* (0, 0, 0)	Sr in 1*a* (0, 0, 0)	Sr in 1*a* (0, 0, 0)
B_{iso} (10^2 nm^2)	0.91(6)	2.38(12)	2.30(10)
	Si in 2*d* (1/3, 2/3, 3/4)		
B_{iso} (10^2 nm^2)	0.43		
	Zn/Si in 2*c* (1/3, 2/3, 1/4)	Zn/Si in 2*c* (1/3, 2/3, 1/2)	Zn/Si in 2*c* (1/3, 2/3, 1/2)
Occ. Zn/Si	1.58/0.42(2)	0.64/1.36(2)	0.33/1.67(1)
B_{iso} (10^2 nm^2)	0.47	0.36	0.64

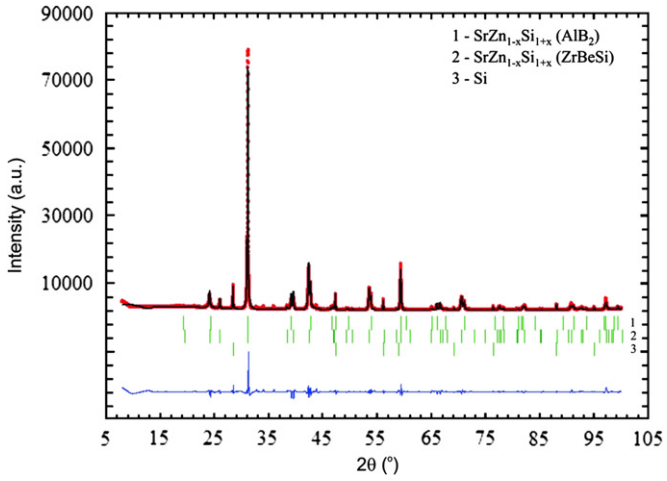

Fig. 7. Rietveld refinement for the alloy with nominal composition $Sr_{33.3}Zn_{21.7}Si_{45}$. The red dots show the observed intensity, the black line the calculated intensity, the blue line represents the difference between measured and calculated intensities, and the green bars indicate the Bragg-positions of each phase. (For interpretation of the references to colour in this figure legend, the reader is referred to the web version of this article.)

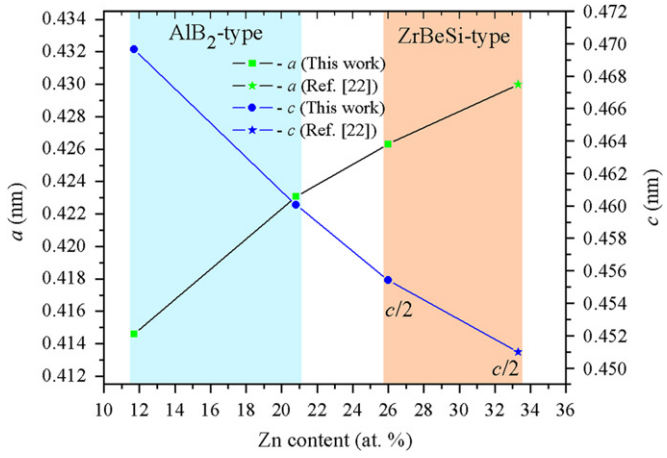

Fig. 8. Lattice parameters versus Zn content for silicides $SrZn_{1-x}Si_{1+x}$ (τ_2 and τ_3) (EPMA data).

in one of the crystallographic sites of these phases were evaluated. In the Sr–Zn–Ge system at 700 °C a new phase with AlB_2 structure was found. All ternaries in this system with exception of the clathrate-I phase $Sr_8Zn_8Ge_{38}$ are characterized by homogeneity regions with statistical mixtures of Ge and Zn in the crystallographic positions.

Acknowledgments

V.V.R. and P.R. are both grateful to the OEAD Austrian – Ukrainian Scientific – Technological Exchange Program "Ernst Mach" for a fellowship in Vienna.

References

[1] N. Melnychenko-Koblyuk, A. Grytsiv, P. Rogl, M. Rotter, E. Bauer, G. Durand, H. Kaldarar, R. Lackner, H. Michor, E. Royanian, M. Koza, G. Giester, Phys. Rev. B: Condens. Matter Mater. Phys. 14 (2007) 76.
[2] N. Melnychenko-Koblyuk, A. Grytsiv, P. Rogl, M. Rotter, R. Lackner, E. Bauer, L. Fornasari, F. Marabelli, G. Giester, Phys. Rev. B: Condens. Matter Mater. Phys. 76 (2007) 195124.
[3] N. Melnychenko-Koblyuk, A. Grytsiv, P. Rogl, E. Bauer, R. Lackner, E. Royanian, M. Rotter, G. Giester, J. Phys. Soc. Jpn. 77 (2008) 54.
[4] A. Grytsiv, N. Melnychenko-Koblyuk, N. Nasir, P. Rogl, A. Saccone, H. Schmid, Int. J. Mater. Res. 100 (2009) 189.
[5] N. Melnychenko-Koblyuk, A. Grytsiv, L. Fornasari, H. Kaldarar, H. Michor, F. Rohrbacher, M. Koza, E. Royanian, E. Bauer, P. Rogl, M. Rotter, H. Schmid, F. Marabelli, A. Devishvili, M. Doerr, G. Giester, J. Phys. Condens. Matter 19 (2007) 26.
[6] N. Melnychenko-Koblyuk, A. Grytsiv, St. Berger, H. Kaldarar, H. Michor, F. Roehrbacher, E. Royanian, E. Bauer, P. Rogl, H. Schmid, G. Giester, J. Phys. Condens. Matter 19 (2007) 046203/1.
[7] N. Melnychenko-Koblyuk, A. Grytsiv, P. Rogl, H. Schmid, G. Giester, J. Solid State Chem. 182 (2009) 1754.
[8] N. Nasir, A. Grytsiv, N. Melnychenko-Koblyuk, P. Rogl, E. Bauer, G. Durand, H. Kaldarar, R. Lackner, H. Michor, E. Royanian, G. Giester, A. Saccone, J. Phys. Condens. Matter 21 (38) (2009) 385404.
[9] I. Zeiringer, MingXing Chen, I. Bednar, E. Royanian, E. Bauer, R. Podloucky, A. Grytsiv, P. Rogl, H. Effenberger, Acta Mater. 59 (2011) 2368–2384.
[10] I. Zeiringer, E. Bauer, A. Grytsiv, P. Rogl, H. Effenberger, Jpn. J. Appl. Phys. 50 (5 Part 3) 05FA01/1–05FA01/4.
[11] I. Zeiringer, N. Melnychenko-Koblyuk, A. Grytsiv, E. Bauer, G. Giester, P. Rogl, J. Phase, Equilibria Diffusion 32 (2) (2011) 115–127.
[12] L.T.K. Nguyen, U. Aydemir, M. Baitinger, E. Bauer, H. Borrmann, U. Burkhardt, J. Custers, A. Haghighirad, R. Höfler, K.D. Luther, F. Ritter, W. Assmus, Y. Grin, S. Paschen, Dalton Trans. 39 (2010) 1071–1077.
[13] L.T.K. Nguyen, U. Aydemir, M. Baitinger, J. Custers, A. Haghighirad, R. Höfler, K.D. Luther, F. Ritter, Y. Grin, W. Assmus, S. Paschen, J. Electron. Mater. 39 (2010) 1386–1389.
[14] H. Zhang, J. Zhao, M. Tang, Z. Man, H. Chen, X. Yang, J. Phys. Chem. Solids 70 (2009) 312–315.
[15] H. Zhang, J. Zhao, M. Tang, Z. Man, H. Chen, X. Yang, J. Alloys Compd. 476 (2009) 1–4.
[16] E. Alleno, G. Maillet, O. Rouleau, E. Leroy, C. Godart, Chem. Mater. 21 (2009) 1485–1493.
[17] M. Christensen, B.B. Iversen, J. Phys. Condens. Matter 20 (2008) 104244.
[18] S. Johnsen, A. Bentien, G.K.H. Madsen, M. Nygren, B.B. Iversen, Phys. Rev. B 76 (2007) 245126.
[19] H. Zhang, H. Borrmann, N. Oeschler, C. Candolfi, W. Schnelle, M. Schmidt, U. Burckhardt, M. Baitinger, J.-T. Zhao, Y. Grin, Inorg. Chem. 501 (2011) 1250–1257.
[20] L. Qiu, I.P. Swainson, G.S. Nolas, M.A. White, Phys. Rev. B 70 (2004) 035208.
[21] N. Nasir, N. Melnychenko-Koblyuk, A. Grytsiv, P. Rogl, G. Giester, J. Wosik, G.E. Nauer, J. Solid State Chem. 183 (2010) 565.
[22] W. Dörrscheidt, H. Schäfer, J. Less-Common Met. 78 (1981) 69.
[23] W. Doerrscheidt, N. Niess, H. Schaefer, Z. Naturforsch. Teil B. Anorg. Chem. Org. Chem. 31 (1976) 890–891.
[24] F. Merlo, M. Pani, M.L. Fornasini, J. Less-Common Met. 171 (1991) 329.
[25] L.G. Akselrud, Yu.N. Grin, P.Yu. Zavalii, V.K. Pecharsky, V.S. Fundamenskii, CSD-universal program package for single crystal or powder structure data treatment//Collect. Abstract of the 12th European Crystallographic Meeting, vol. 3, Nauka, Moscow, 1989, p. 155.
[26] T. Roisnel, J. Rodriguez-Carvajal, WinPLOTR: a Windows tool for powder diffraction patterns analysis, in: Proceedings of the EPDIC7, Mater. Sci. Forum 378–381 (2001) 118–123.
[27] L.M. Gelato, E. Parthé, J. Appl. Crystallogr. 20 (1987) 139.
[28] Pauling File Binaries Edition, Version 1.0, ASM International, Materials Park, OH, USA, release 2002/1.
[29] A. Palenzona, M. Pani, J. Alloys Compd. 373 (2004) 214.
[30] R. Nesper, F. Zürcher, Z. Kristallogr. New Cryst. Struct. 214 (1999) 21.